ELSEVIER

Progress in Surface Science 74 (2003) 3–24

Progress in SURFACE SCIENCE

www.elsevier.com/locate/progsurf

Surface diffusion by adsorbate density fluctuation measurements

Janusz Beben [a], Yuri Suchorski [b,*]

[a] *Institute of Experimental Physics, Wroclaw University, pl. Maxa Borna 9, PL50-204 Wroclaw, Poland*
[b] *Chemisches Institut, Otto-von-Guericke-Universität Magdeburg, Universitätsplatz 2, D-39106 Magdeburg, Germany*

In memoriam Professor Maria Stęślicka

Abstract

In this review, we present a detailed study of the surface diffusion of adsorbed atoms and molecules on metal surfaces via the analysis of adsorbate density fluctuations in nanosized adsorption systems. Three different experimental approaches, all based on field emission techniques are presented: measurements of field emission current fluctuations, the analysis of local brightness fluctuations of digitized field emission images and the analysis of field ion rate fluctuations.

Keywords: Field emission microscopy; Field ion microscopy; Surface diffusion; Density fluctuations

1. Introduction

One of the most impressive manifestations of the mobility of adsorbed atoms and molecules on surfaces is the spontaneous build-up and decay of microscopic concentration deviations from equilibrium in an apparently homogeneous adsorbed layer. As a result of these fluctuations, the snap-shot of the local adsorbate density distribution would exhibit certain microscopic concentration profiles. Surface diffusion (SD) parameters can be derived from the study of the time evolution of these concentration inhomogeneities (as it can be done for the macroscopic concentration profiles [1]), provided the applied technique is powerful enough to monitor the adsorbate density fluctuations (DFs). The physical basis for such an approach is

* Corresponding author. Tel.: +49-391-671-8824; fax: +49-391-671-1396.
E-mail address: yuri.suchorski@vst.uni-magdeburg.de (Y. Suchorski).

0079-6816/$ - see front matter
doi:10.1016/j.progsurf.2003.08.002

Onsager's hypothesis, which states that the microscopic DF decay in the hydrodynamic regime is in accord with macroscopic laws [2].

The field emission microscope (FEM) is a naturally suitable technique for the monitoring of the adsorbate DFs, since it combines both relevant prerequisites: high spatial resolution and the necessary coverage-sensitivity. The idea about the usefulness of the field emission current-noise, as the origin of information about the surface mobility of adsorbed species, was expressed already in the 1960s by Kleint and Gasse [3], although the direct relation between the noise in the electron emission and adsorbate DFs was not considered yet. This relation was found by Gomer [4] by measuring the autocorrelation function (AF) of the local adatom-concentration in a probe–hole experiment. Due to the high magnification of the FEM, the electrons emitted from the surface area of ca. 10 nm radius (RMS fluctuations from the mean particle number range then within a few percent) can be collected by a probe–hole of 1 mm radius in the screen. The exponential dependence of the field emission current on the work function changes, caused by the adsorbate density deviations, allows the reliable monitoring of the fluctuations. The characteristic decay time of the microscopic concentration inhomogeneties τ, derived from the AF, is related to the diffusion coefficient D by $\tau = r_0^2/4D$ where r_0 is the radius of the probed surface area.

In the last decades, a number of interesting and quite unexpected results has been obtained using the different modifications of the method [5], including the analysis of the local brightness fluctuations of the digitized field emission images [6]. The last approach is based on the idea of the "virtual probe–hole", a "region of interest" (ROI which corresponds to an area of a few nm^2 on the tip surface) cut out in the digitized FEM video-frames. The idea to analyse the digitized FEM video-record of the fast surface processes results, in turn, from the increasing interest to platinum and rhodium field-emitter tips as model catalysts. Because of their structurally heterogeneous surface, such tips represent well the complex structure of the metal catalytic particles of the supported catalyst. The surface of a field-emitter tip can be prepared reproducibly and characterized with atomic resolution by field ion microscopy (FIM). With FEM one can then follow the dynamics of the surface processes with a lateral resolution of $\sim$2 nm and visualize in situ the surface reaction (e.g., catalytic CO oxidation) on such well defined nanosized facets [7]. The role of the atomic steps, size effects and microscopic fluctuations can be studied in this way [8]. It is tempting to investigate the diffusion processes in the reaction conditions, especially due to the important role of the diffusive coupling in the reaction. The DF method would be highly suitable for this purpose, provided the FEM video-records can be analysed in respect thereof.

In this review, we present three different experimental extensions of the DF method, all based on the FEM techniques including a successful attempt to analyse the local brightness fluctuations of the digitized field emission images, as well an example of the analysis of the field ion rate fluctuations in the FIM.

2. Experimental realization

The conventional probe–hole technique, employed by Gomer in the early experiments, established the SD measurements using the autocorrelation function for

the field emission current fluctuations. The current fluctuations can be, with the corresponding calibration, related to the fluctuations of the number of adatoms N in the probed area, whose autocorrelation function is $A_N(t) = \langle \delta N(t+t')\delta N(t')\rangle_{t'}$, where $\delta N(t)$ is the fluctuation of N at time t and $\langle\ \rangle_{t'}$ denotes average over t'. The AF is, in the hydrodynamic regime, related to the diffusion coefficient through the equation

$$A_N(t) = (\langle N\rangle/A)\int_A (1/4\pi Dt)\exp(-|r-r'|^2/4Dt)drdr', \tag{1}$$

where the integration over r and r' proceeds over the entire area A [9]. A semilog plot of the experimentally obtained AF is then compared with the theoretical curve derived from Smoluchowski's theory of DF which was developed for independent particles in 1914 [10]. The diffusion coefficient D is obtained from the comparison. The time Fourier transform of the function $A_N(t)$ represents the spectral density function $W(\omega)$ which is in most cases much more easily to interpret. The selected components of $W(\omega)$ can be also measured directly [11].

The most direct way of studying SD by fluctuation method is the cross-correlation approach initiated by Kleint and coworker [12]. The idea consists in the cross-correlation analysis of fluctuations that occur in two neighbouring areas A and B separated by the distance Δ. The corresponding cross-correlation function is defined as

$$CC(t,\Delta) = \langle \delta N^{\mathrm{A}}(t+t')\delta N^{\mathrm{B}}(t')\rangle_{t'}, \tag{2}$$

where δN^{A} and δN^{B} are the fluctuations in the regions A and B, correspondingly. For the hydrodynamic fluctuations the cross-correlation function $CC(t,\Delta)$ can be derived as

$$CC(t,\Delta) = 1/A\left\{\int_{\mathrm{A}} d^2r\left\{\int_{\mathrm{B}} d^2r'(\exp(-|r-r'|^2/4Dt))(1/4\pi Dt)\right\}\right\}, \tag{3}$$

where the integral is calculated over the both probe regions A and B, for the detailed analysis see [13]. It can also be shown that in the hydrodynamic regime the cross-correlation function may exhibit a maximum which can be well approximated by Smoluchowski's theory [14].

The corresponding experimental arrangement of the "two probe–hole" FEM fluctuation experiment by Beben et al. [15] is shown in Fig. 1. In this experiment, the fluctuations are measured by use of two "slit"-like probing collectors. These correspond to a probing area of ca. 5×30 nm^2 each. The probing distance between them varies from 30 to 70 nm. Adjusting the tip in respect to the slit-like collectors allows to chose a fixed surface area of interest on the tip apex. Rotating the tip enables additionally the SD-anisotropy to be studied using the singular slit-like probe–hole, since the fluctuations obviously decay faster across the short side of the probing area than across the long one. The formal way of the SD-tensor determination using the slit-like probing region was presented by Bowman et al. [16].

First, we present the spectral density results for the potassium atoms adsorbed on the W(1 1 2) facet obtained by the singular circular probe–hole (Fig. 2(a)). The

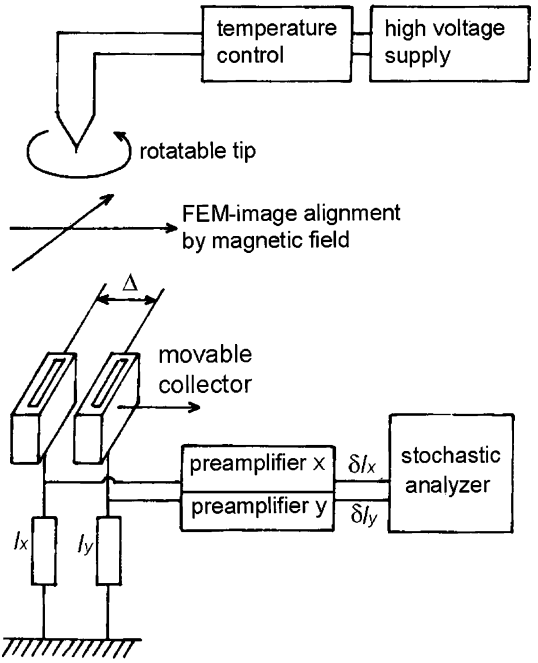

Fig. 1. Schematic diagram of the experimental setup for the cross-correlation measurements of the field emission fluctuations. Version with the slit-shape collectors is shown. Taken from [15].

experimental points and the theoretical curves calculated for a circular probe region are superimposed and the diffusion coefficient is obtained. The temperature dependence of the diffusion coefficient is depicted in an Arrhenius plot (Fig. 2(b)) which serves for the determination of the SD activation energy. The coverage dependence of the activation energy for the diffusion of potassium in the submonolayer on W(1 1 2) is displayed in Fig. 2(c). The "oscillation behaviour" of the coverage dependence of the SD activation energy for the alkali adsorbates, which is easily visible in Fig. 2(c), is discussed in Section 3.1.

The results obtained using the singular slit-like probe are presented in Fig. 3(a)–(c), where the angular dependence of the diffusion coefficient (Fig. 3(a)) in a polar coordinate diagram is shown and an example of the Arrhenius plot for one chosen direction is shown (Fig. 3(b)). The anisotropy of the SD activation energy, in turn, displayed in Fig. 3(c).

The cross-correlation results, measured with the two-slit collector assembly, are shown in Fig. 4(a)–(c). In accord with the theoretical predictions, they reveal a distinct maximum which depends on both the distance Δ between the probe regions and the sample temperature T. The time delay corresponding to the maximum, τ_m, increases with the distance Δ. Fig. 4(b) shows the dependence of the τ_m on the square distance at a temperature of 400 K and a potassium coverage of $\Theta = 0.35$.

Assuming that the distance between the probed regions Δ is much greater than their size, we may expect from the theory to find the cross-correlation maximum at

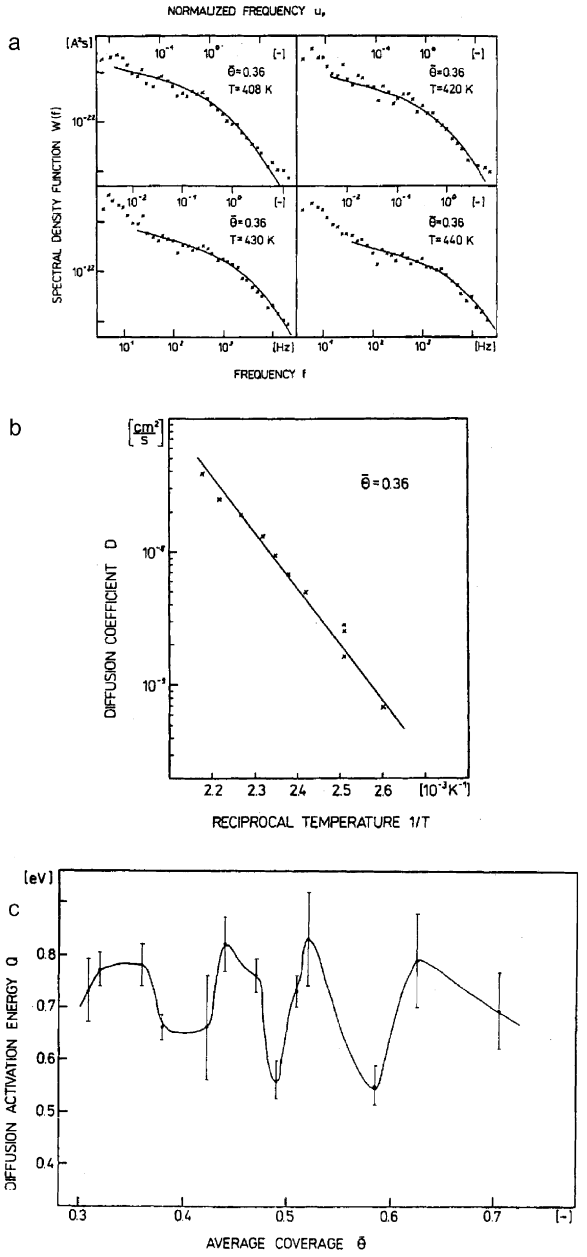

Fig. 2. Spectral density results: (a) experimental spectral density functions for the potassium adlayer on the W(1 1 2) facet at coverage $\Theta = 0.36$ in temperature range from 408 to 440 K. Solid lines are theoretical curves for two-dimensional diffusion, crosses are experimental points; (b) example of an Arrhenius plot for same coverage and (c) coverage dependence of activation energy of diffusion for the same adsorption system. (a)–(c) are taken from [25].

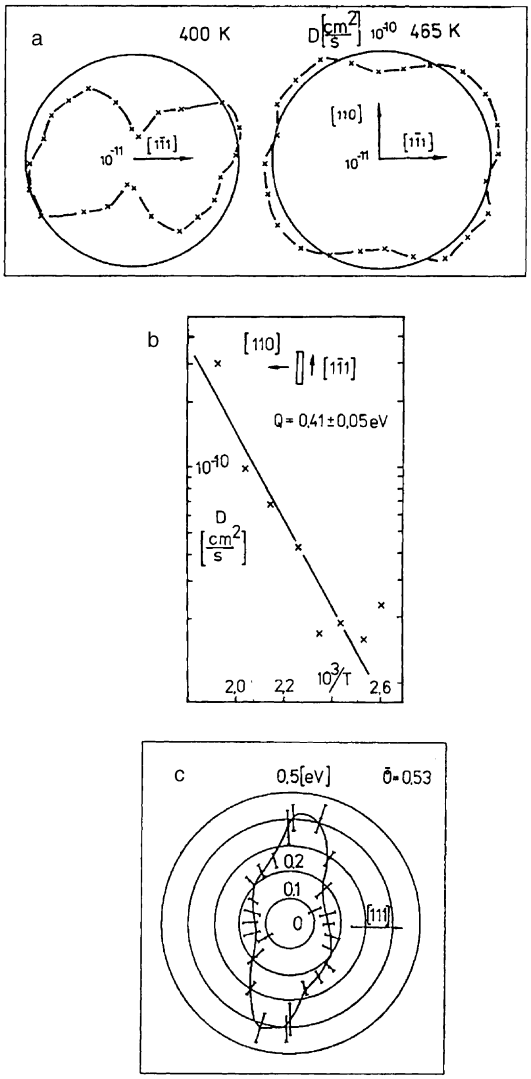

Fig. 3. Anisotropy of potassium diffusion on W(1 1 2)-facet at coverage $\Theta = 0.53$: (a) angular dependence of diffusion coefficient obtained by the slit-like collector. Crystallographic directions along W(1 1 2) are indicated; (b) example of an Arrhenius plot for a slit-like probe region placed on W(1 1 2)-facet. The Position of the slit-probe–hole in respect to crystallographic directions is indicated schematically by vertical and horizontal arrows [17] and (c) activation energy of surface diffusion in polar coordinate diagram. Bars correspond to experimental errors.

the Gaussian curve describing Smoluchowski's "aftereffect" which is approximated by the formula

$$CC(t, \Delta) \approx (4\pi Dt)^{-d/2} \exp(-\Delta^2/4Dt), \tag{4}$$

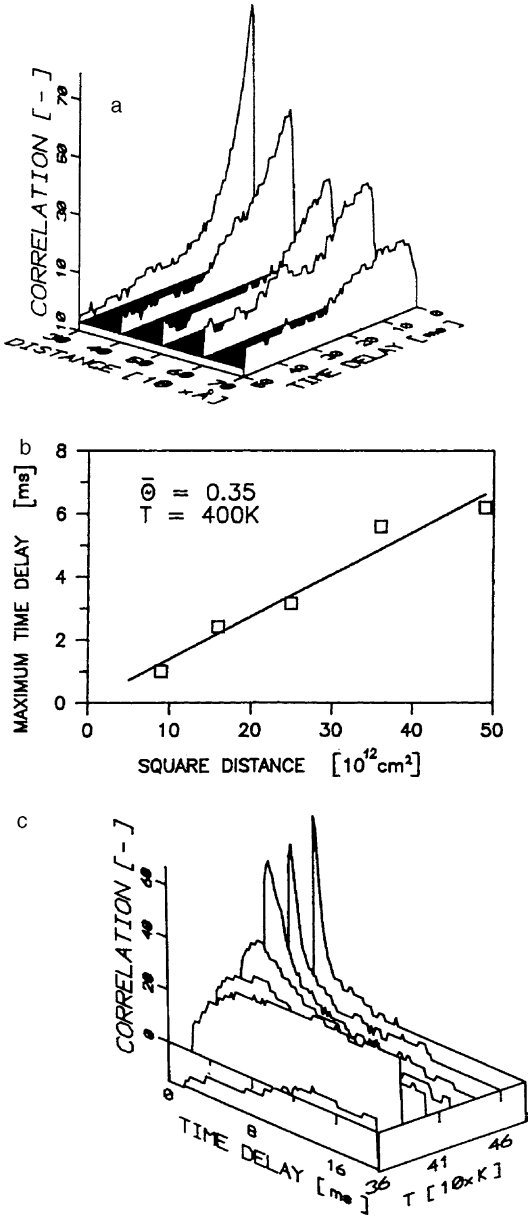

Fig. 4. Cross-correlation data measured using the two-slit collector assembly for the K/W(1 1 2) adsorption system: (a) evolution of the cross-correlation functions with the increasing distance between the probe regions. Both slit-like collectors were placed perpendicularly to the [1 1 1] direction on the W(1 1 2) facet. Potassium coverage $\Theta = 0.35$; (b) time delay maximum vs. square distance for the cross-correlation functions shown in (a) and (c) the same as in (a) but for the potassium coverage of $\Theta = 0.38$. The curve for $T = 360$ K reveals negative values in a large range of the time delay [17].

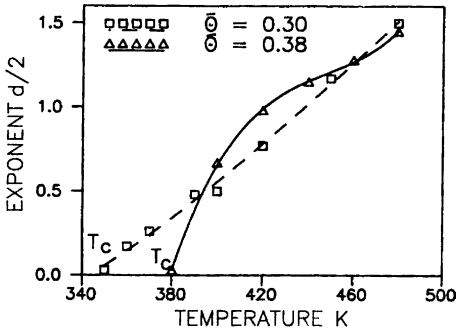

Fig. 5. Temperature dependence of the exponent $d/2$ (Eq. 4) for two different coverages $\Theta = 0.30$ (triangles) and $\Theta = 0.38$ (crosses). The temperatures at which the parameters approach zero are marked on the diagram by T_c [17].

where d is the dimensionality of the system [17]. Unfortunately, the experimental results deviate somewhat from the theoretical predictions. Namely, the experimental cross-correlation functions show a slower decay with decreasing temperature and cannot be fitted by (4) keeping $d = 2$ as for the two-dimensional system. A Monte Carlo (MC) procedure was applied and the parameters D and d were estimated to achieve the best fitting to experimental data. A reasonably good agreement with the experiment was obtained and the temperature dependence of the parameter d could be determined. Fig. 5 presents the results for potassium coverages of $\Theta = 0.30$ and of $\Theta = 0.38$ and for the same distance $\Delta = 30$ nm. The temperatures at which the parameters approach zero are marked on the diagram by T_c. Below T_c the cross-correlation functions become negative (see, e.g., the cross-correlation function for 360 K in the Fig. 4(c)) and, thus, the described procedure is not applicable anymore. We discuss the physical meaning of T_c in the Section 3.3.

3. Achievements and problems

The large number of experimental data obtained by the FEM–DF method is still not fully explained, since some of the surface phenomena generating the FE-current fluctuations are not handled sufficiently in the theory. The example of prediffusion [18,19] is known best. The diffusion model of fluctuations in AF-terms is most developed. The principles were given by Gomer [4] and the extension of it for the investigation of anisotropic diffusion was done by Bowman et al. [16]. The autocorrelation measurements were successfully used in the examination of diffusion of such adsorbates as CO [19], oxygen [9] and hydrogen [20,21] on tungsten surfaces. Interacting adatoms were examined in AF-terms by Read and Ehrlich [22] who used MC simulations. The detailed diffusion model in terms of the spectral density function was elaborated by Timm and van der Ziel [23], the extention of this model by Gesley and Swanson [24] considers both the effect of the boundaries and the

anisotropic diffusion. We follow the approach of [24] in our interpretation of the spectral density results.

3.1. Structure of spectral densities

The shape of the spectral density functions derived from FEM experiments has not been clear for a long time. A large number of experimental results showed different structures for the spectral densities, as, e.g., data in [25], which were not understood and were even a reason for the early criticism of the diffusion mechanism [26,27]. The considerable progress in the theory of field emission current fluctuations during the last decade provides now a better understanding of many results obtained in the past, such as in [28]. To understand the structure of the spectral densities, two effects which influence the low frequency range should be taken into account. The first is the effect of bounded diffusion which leads to the increase of the slope $dW(\omega)/d\omega$, but which should be temperature independent. [24], and the anisotropy of diffusion, which, in turn, depends on temperature [17]. Both effects overlap and are difficult to separate. For the adsorption system potassium on tungsten, which is discussed here, these effects are expected to appear as well. On one side, the dimension of a single crystal facet of our tip-specimen is comparable with the size of the probe regions, and, on the other, direct observations of single adatoms by FIM show that the boundaries of planes may reflect the adatoms in their diffusion motion [29]. Potassium atoms deposited on tungsten reveal a strong mutual dipole-dipole interaction and LEED experiments have shown that adlayer superstructures are created even at a very low coverage [30]. This may lead to anisotropic diffusion. The MC modelling by Sadiq and Binder [31] has shown a quasi one-dimensional behaviour for a square lattice where the (2×1) surface structure occurred. The effect is more pronounced if the substrate plane is anisotropic as it is in our case of the (1 1 2) plane of tungsten. All this suggests that for the considered adsorption system the structure of the spectra should be, in general, temperature dependent.

Our experimental spectra for K/W(1 1 2) and K/W(1 1 1) systems confirm the theoretical predictions [24]. Indeed, the conclusion that the shape of the spectra for the W(1 1 1) surface results from the bounded diffusion (compare Figs. 2(a) and 6, right side) can be drawn from the comparison of the spectra for the W(1 1 2) and W(1 1 1) planes. The observed effect is certainly complex. The (1 1 1) crystal plane of our W tip is a very small facet surrounded by terraces. The larger neighbouring facets such as (1 1 2) planes can, to same extent, act as a boundary for diffusing adatoms causing the occurrence of the flat part in the corresponding spectrum (Fig. 6, right side).

The spectra for the (1 1 2) plane can result again from both the effects of boundary diffusion and anisotropy. The W(1 1 2) facet is a highly anisotropic plane and at the same time it is also confined by the reflecting boundaries. The "two-dimensional" spectra obtained in this case may well be a superposition of both effects. At low temperatures the shape of the spectral density functions changes in the low frequency range. This can be explained by anisotropic diffusion: at low temperatures adatoms adsorbed on the W(1 1 2) surface mostly move in the [1 1 1] direction and the

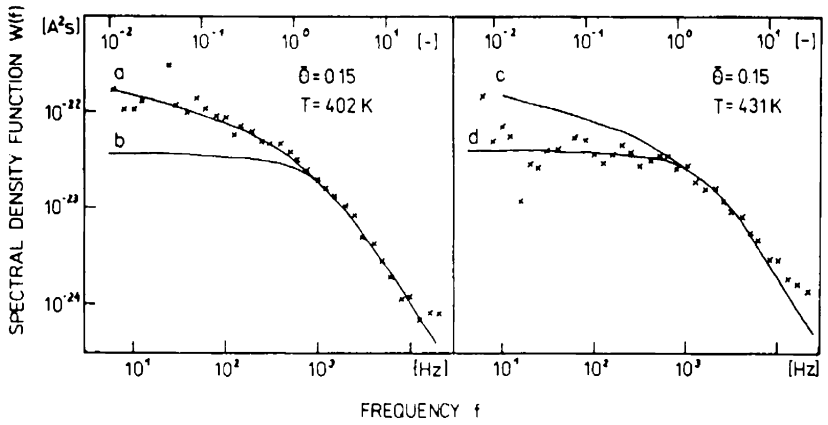

Fig. 6. Shape-evolution of the spectral density curves for the K/W(111) system ($\Theta = 0.15$) with increasing temperature. Crosses are experimental points. Curves *b* and *d* are theoretically calculated bounded (*a* and *c* unbounded, correspondingly) diffusion spectra [15].

one-dimensional diffusion predominates. The corresponding transition from the two-dimensional to the one-dimensional diffusion at decreasing temperature is shown in Fig. 7.

The activation energies for diffusion presented in Fig. 2(c) were calculated for the high temperature range where the structure of the spectral densities does not change much anymore. The results refer to the circular probe region and, therefore, the obtained diffusion coefficients and the activation energies are directional averages. The maxima and minima of the "oscillation behaviour" may reflect the influence of different surface structures formed by the adsorbate atoms and are related to the varying symmetry of the two-dimensional structures and their orientation (commensurate/incommensurate layers). Both depend on temperature and coverage. The varying different lateral interaction in such layers and the different degree of the "fitting" to the substrate-structure significantly influences the diffusivity of the adatoms [32]. Similar changes of the noise power with coverage were also observed for lithium adsorbed on the W(1 1 2) plane [33] and a correspondence between minima and coherent structure, known from LEED experiments [34], has been found.

3.2. Anisotropy of diffusion

Anisotropy of diffusion has been examined using the DF method both theoretically [1,16] (also using the MC simulations [35]) and experimentally by the slit collector with subsequent analysis of the AF [5,20]. Herewith we extend this approach to the analysis of the spectral density function, again for potassium on tungsten, using the W(1 1 2) facet as a probing surface which furrowed relief makes this plane very suitable for examining the SD anisotropy. Because of the furrows, the diffusion is quasi one-dimensional (along the furrows) at low temperatures, at increasing temperature a "two-dimensional" motion of adatoms is expected. This expectation is

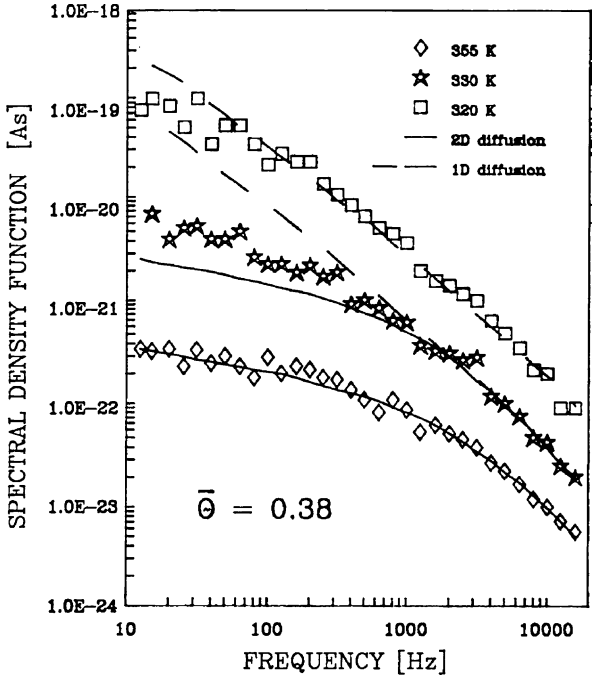

Fig. 7. An example of the transition from one- to two-dimensional diffusion for the circular collector, the W(1 1 2)-facet and potassium coverage $\Theta = 0.38$. Squares. Stars and diamonds are experimental points. The dashed and solid lines are theoretical spectral densities for one- and two-dimensional diffusion, respectively. The curves corresponding to 330 and 320 K are shifted by one and two decades, respectively, for better viewing relative to that for 355 K [17].

supported by the values of the diffusion coefficients presented in a polar coordinate diagram which can be seen in Fig. 3(a) or by the activation energies presented in Fig. 3(c).

The diagrams, in general, reveal the expected trend, but details of the angular dependence of the diffusion coefficient are surprising. The maximum of the diffusion coefficient shows a certain deviation from the [1 1 1] direction. A tentative explanation of this phenomenon could be that the deviation results from the adlayer structure itself [17].

3.3. Phase transition observations

The DF method was first applied to the occurrence of a second order phase transition by Mazenko [36]. An interacting adsorption system was considered and the AF at the transition temperature was derived for the long-time limit as $A(\tau) \sim \tau^{-\eta/z}$, where η and z are critical indices. This means that, when the system enters the critical region tending to the critical temperature T_c, the long-time tail of the AF should "cross over" from τ^{-1} to $\tau^{-\eta/z}$. At the critical temperature T_c, the value

of $d/2$ should be 1/15, assuming the Ising model. The cross-correlation should have the same behaviour because the long-time limit is geometry independent. This idea was extended by Shikhovtseva et al. [13] to both the cross-correlation and spectral density functions. Fig. 8 shows the corresponding cross-correlations for both hydrodynamic and critical fluctuations plotted after numerical calculations. The calculated curves for $m = 0$ (m is the ratio of the distance between patches and patch radius) correspond to the AFs. The distance dependence of the cross-correlation (spatial correlation) can be also expressed analytically and is shown in Fig. 9. For hydrodynamic fluctuations, the overlapping patches only give non-zero correlation ($m = 2$ correspond to the adjacent patches). For critical fluctuations, the cross-correlation is always positive and decays with the distance between patches as $x^{-1/4}$ These calculation can be useful when interpreting experimental data. For hydrodynamic fluctuations, the correlation functions decay as t^{-1}. A slower decay may indicate that we are inside a critical region. Another characteristic feature of critical fluctuations is a positive value of the cross-correlation at $t = 0$ (for separated probe-regions) that should be zero for hydrodynamic fluctuations.

Fig. 5 shows the temperature dependence of the exponent $d/2$ which tends to ~ 0 with decreasing temperature. The value of 1/15 obtained theoretically for the decay of the cross-correlation at the critical temperature is contained within the experimental error. To quote [36], the second-order phase transition occurs and the critical temperature T_c is about 350 and 380 K at coverages of 0.30 and 0.38, respectively. Below T_c, the above procedure does not work. The cross-correlation assumes negative values and cannot be fitted by a Gaussian. The observed second-order phase transition is of the order-disorder type. This is also manifested by the variation of the low-energy diffraction patterns. The experimental results, as well as the MC experiments, show that the critical temperature is strongly coverage dependent and increases with increasing coverage [37,38]. These are in agreement with the results achieved by the fluctuation method (cf. Fig. 5). The critical temperature that results

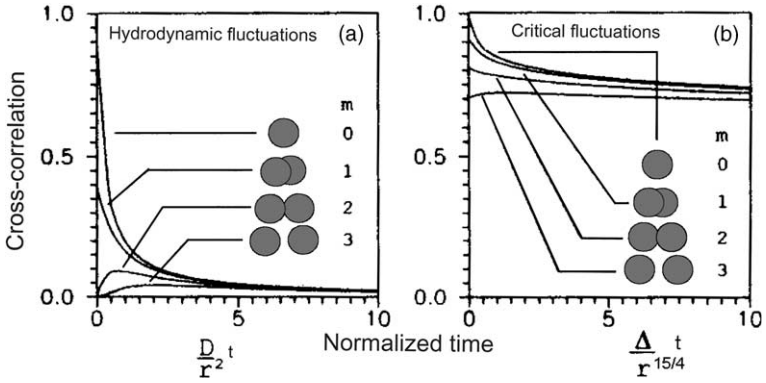

Fig. 8. Calculated cross-correlation functions for the hydrodynamic (a) and critical (b) fluctuations. The probed region geometry is shown inside the diagrams. Parameter m is the ratio of the distance between patches and patch radius [13].

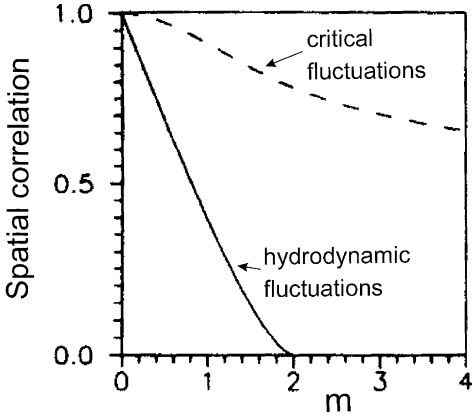

Fig. 9. Distance dependence of normalized cross-correlation function at $t = 0$ (spatial correlation function). Solid and dashed lines correspond to hydrodynamic and critical fluctuations, respectively. The meaning of m is the same as in Fig. 8 [13].

from the temperature dependence of the LEED spot intensity for potassium adsorbed on Mo(1 1 2) is related to the c(2×2) surface structure at about 350 K [39].

4. Surface diffusion measurements from digitized FEM images

The conventional FE probe–hole technique, described in the previous sections, uses only a fixed area of an average size of about 20×20 nm^2 (or two such areas in the case of cross-correlation measurements) for monitoring local FE current fluctuations, neglecting all the information contained in the rest of the FEM image. The digitization of the FEM images makes this information available. First attempts of computer-processing of FEM images are dated to the early ninetees, when the "digital" field emission microscope was developed by van Tol et al. [40]. Later, the digitization of the FEM-images was used to study the oscillations in catalytic CO-oxidation reaction on Pt [41]. Suchorski et al. [6,42] proposed to use this approach for studying DFs on the basic of the fact that local brightness variations of the FEM image follow the adsorbate DF via the associated work function changes [23].

The time resolution is restricted to that of the image-recording process (e.g., 40 ms/frame in the case of conventional video-technique) and, therefore, one has to chose a suitable system which provides sufficient variations of the local intensity of the FEM image and a corresponding diffusivity range. We have selected Li on a Pt field emitter to demonstrate the applicability of the proposed method.

The FEM video-images of the Li-covered [1 0 0] oriented Pt-tip surface (Li coverage of 2.5×10^{14} cm^{-2}) were digitized with 8-bit resolution. Certain rectangular areas (ROIs) were set, whose height, width, orientation and location could be chosen arbitrarily. The intensity was integrated for each ROI following, in general, the procedure described in [41]. Since this can be done frame-by-frame, the fluctuations of the intensity for each particular ROI can be monitored. Such a ROI can be

considered as a "virtual probe–hole" corresponding to a certain probed surface region of nanometer size. The size of the region probed by such a "virtual probe–hole" can be estimated by overlapping the FEM image containing the chosen ROIs with an atomically resolved low-temperature Ne-FIM image of the same tip. Typically, the size of the probed area varied in the range between 10×10 nm^2 and 22×22 nm^2 in the present study.

The advantage of this method is that several separate, contacting and even overlapping "virtual probe–holes" can be placed simultaneously in different regions of the image, a procedure which is not possible with the "real" probe–hole technique. Additionally, a slit-like "virtual probe–hole" (a stripe across the FEM image corresponding to a 20 nm wide probed area on the surface) was set, in which the *intensity profiles* (intensity integrated across the stripe vs. distance along the stripe) were measured frame-by-frame. From the intensity profiles, the cross-correlations for different parts of the stripe were calculated. Such a "virtual slit probe–hole" can also be rotated within the digitizing procedure thus allowing in principle the SD anisotropy to be studied as was shown for a real slit-like probe–hole in Section 2. More details of the digitization can be found elsewhere [41,42].

Fig. 10 shows the examples of the experimental AFs for the "virtual probe–hole" fluctuations recorded in the FEM video-images of our Li/Pt(1 0 0) system. The corresponding theoretically calculated AFs, all fitted to the experimental curves for four different sample temperatures, are also shown. The use of a recursive numerical band filter can lead to the appearance of the minor oscillation-like variations in the curve tail. These low-magnitude oscillations, however, do not influence the diffusion parameters obtained from the non-oscillating initial part of the AFs.

The temperature dependence of the diffusion coefficient (Arrhenius plot), derived from the AFs is presented in Fig. 11. The slope of this dependence yields a value of

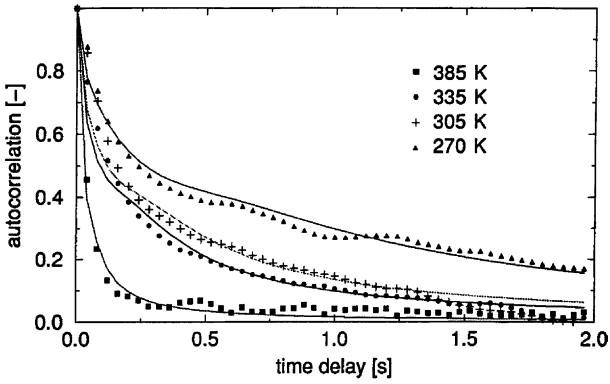

Fig. 10. Normalized autocorrelation functions for local ("virtual probe–hole") fluctuations in the FEM image of the Li submonolayer ($n_{Li} = 2.5 \times 10^{14}$ cm^{-2}) on apex plane of the [1 0 0]-oriented Pt tip. Size of probe region on the surface was 22×22 nm^2 as estimated from the corresponding Ne FIM image. Dots of various shapes represents experimental values; Solid lines are fitted theoretical autocorrelation functions [42].

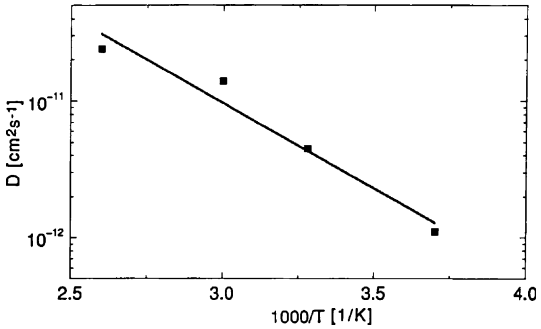

Fig. 11. Temperature dependence (Arrhenius plot) of the diffusivity D of Li adatoms in the Li submonolayer ($n_{Li} = 2.5 \times 10^{14}$ cm^{-2}) on the stepped Pt(1 0 0) surface. Activation energy value obtained from this slope is $E_{act} = 0.25$ eV [42].

0.25 eV for the activation energy of Li SD on a stepped Pt(1 0 0) surface at Li coverage of 2.5×10^{14} cm^{-2}.

In the cross-correlation analysis, the fluctuations in two "virtual probe–holes" separated by a distance of few nm are investigated. Some examples of the normalized cross-correlation functions obtained from the same FEM video-sequences, as in Fig. 10, are displayed in Fig. 12. For two of four chosen separations, ranging from 0 to 20 nm, the cross-correlation function reveals a distinct maximum as predicted, which depends on the probed regions separation. This result confirms the applicability of the hydrodynamic description of adsorbate density fluctuations in present case of Li submonolayer on Pt(1 0 0). Using the cross-correlation approach described in Section 2, the diffusion coefficient can be found from τ_m, the time delay corresponding to the maximum. The τ_m value of 0.08 s read from Fig. 12 yields the diffusivity of about

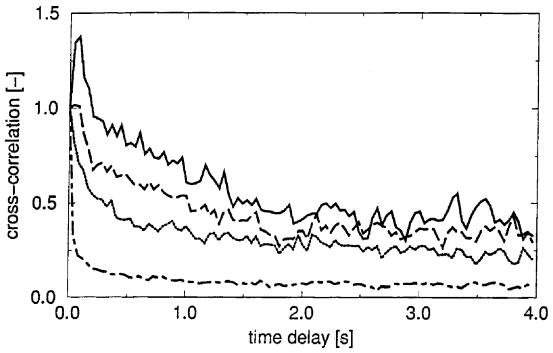

Fig. 12. Normalized cross-correlation functions obtained experimentally from intensity profiles of the same FEM video-images as in Fig. 10, for four chosen separation distances Δ at 380 K. Solid line corresponds to $\Delta = 20$ nm, dashed line to $\Delta = 15$ nm, dotted line to $\Delta = 10$ nm, dashed-dotted line to $\Delta = 0$ (autocorrelation). Diffusivity obtained from the solid line curve (separation 20 nm) $D = 1.2 \times 10^{-11}$ cm^2 s^{-1} [42].

1.2×10^{-11} cm^2 s^{-1}, in agreement with the values obtained from the AF at similar temperatures of the tip (380 K). It is to be noted, that in the present case the maximum of the cross-correlation is detectable at somewhat larger distances as compared to the theoretical predictions [13]. In our opinion, the reason for this is (at least partially) the finite resolution effect described in [43].

In discussing the present results on the SD of Li on the Pt(1 0 0) tip-facet, one should take into account that the potential barrier for the Li SD in this case is mainly governed by the structure of the atomic steps present on the apex of a [1 0 0]-oriented Pt-tip. Therefore, the SD data obtained for the field-emitter facets have to be compared with caution with the data measured for the macroscopic single crystals. Additional problems can appear due to applied field of 3–5 V/nm in FEM, which influences in principle slightly the SD of Li on the solid surfaces [44]. The eventual field effect is, however, not the peculiarity of the DF measurements, but is a general feature of the FEM approach. Unfortunately, the surface diffusion of Li, has so far not been studied on Pt(1 0 0) single-crystal surfaces and Pt field emitters. Nevertheless, we can compare qualitatively the present data with the recent results of Snitko [45] for Li-submonolayers on a Mo-tip. Values of D of the order of 10^{-11}–10^{-10} cm^2 s^{-1} ($T = 286$ K) and of E_{act} of 0.2–0.3 eV were obtained in [44] from the spreading of the Li in a concentration gradient created by Li field desorption from the apex of a [1 0 0]-oriented Mo tip. Similar values of D (10^{-10}–10^{-9} cm^2 s^{-1} at 400 K) and of E_{act} (0.4 eV) were obtained for the SD of Li in the coverage range from 1.3×10^{14} to 2.8×10^{14} cm^{-2} on different facets of a [1 0 0]-oriented W tip with the field-emission fluctuation method [46].

From the cross-correlation data the "signal transmission velocity" can be determined, that characterises the time necessary for the transmission of the signal (in present case the local deviation from the average surface density) through the system [47]. From the distance between the probed regions and from the maximum of the cross-correlation function the value of 10^{-5}–10^{-4} cm s^{-1} can be read. The method can also be applied for studying the signal transmission velocity in chemical-wave propagation, such as was observed during in situ FEM/FIM visualisation of the catalytic surface reactions, e.g., CO oxidation on Pt [7]. Recent employment of the "virtual probe–hole" served for the discrimination of the reaction-induced fluctuations on the active branch of the catalytic CO oxidation from the rather diffusion-induced ones on its inactive branch [6,8], and allowed the detection of the noise-induced transitions near the bifurcation point of the reaction [48].

5. Field ion rate fluctuations and diffusion

It is challenging to apply the DF experimental approach in the FIM mode. Unfortunately, despite recent progress in revealing details of the localized field ionization [49], the interpretation of current fluctuations for field ions still remains more complicated than for field electrons. However, for an imaging gas such as CO, whose field-desorption mechanism of ionization has recently been revealed [50], we can relate the locally registered CO^+ ion rate to the number of CO molecules arriving at

the probed surface sites during the sampling time there. With this assumption, we conclude that fluctuations in the number of desorbed CO^+ ions reflect fluctuations in the diffusion flux of CO molecules towards the probed sites. Thus, the theory of DF can be applied to determine the diffusion coefficient.

We present here the results of the first attempt of an autocorrelation analysis of rate fluctuations of CO^+ field ions emitted from W(1 1 1) [51]. The apparatus used for the registration of field ion rate fluctuations was the same as we used for the probe–hole retarding potential analysis of CO^+ field ions [50,52]. The CO^+ field ion beam, emitted from the apex plane of the [1 1 1]-oriented W tip and focused by tube lenses, passes a 60° magnetic sector field for mass-to-charge separation and finally enters the retarding-potential analyzer equipped with an electron multiplier for single particle detection. The field ion rate was recorded with a 1024 channel analyzer using a sampling time of 0.05–0.1 s. The whole instrument working under UHV conditions was connected to a gas inlet system by which CO and He (used for tip preparation) of the highest available purity were introduced. The experimental details have been described elsewhere [50,52].

Before obtaining the experimental AFs, the probed signal was passed through a recursive numerical band filter with cut-off frequencies at 0.05 and 1 Hz. This procedure was necessary to dump trends and high frequency components. Fig. 13(a)–(c) show three examples of theoretically calculated AFs, all fitted to the corresponding experimental curves for the tip temperatures of 130, 155 and 182 K. The decay of the AFs tends to diminish with decreasing temperature, indicating progressively increasing ordering in the adsorption system [13,16,36].

An estimate of the size of the region probed by the diffusing particles, necessary for determining the diffusivity, was made from an evaluation of the spatial zone from which most CO molecules are supplied to the ionization zone. The size of the area around the top of the tip, where the molecules are mainly collected from the gas phase, depends on the field distribution and the temperature of the tip. We performed numerical calculations of the asymptotic field distribution and of the field enhancement of the gas-kinetic flux of CO towards the tip surface as well as of the effective CO collection area. The calculations are based on general considerations of the gas supply in an FIM developed by Southon [53]. A sphere-on-cone model [54] was used for a more realistic tip-form approximation than the spherical model used in [53]. The corresponding results are shown in Fig. 14, where both the dependence of the CO gas-kinetic flux toward the surface, and of the effective (accounting for field-enhancement of the CO flux) CO-collecting surface area on the distance from the top of the tip, are displayed. The limits of the trapping zone for two particular temperatures of 120 and 190 K and constant applied field of 20 V/nm are also indicated. Details of the model itself and numerical estimations are given in [54]. As follows from Fig. 14, the CO collection area effectively extends up to 5 tip radii, i.e. the average distance probed by diffusing CO molecules is about 250 nm for the tip used in the present experiments. For every given temperature and field value, a corresponding probing distance was estimated. The characteristic time for the supply zone formation was about 0.1 s, as obtained from an analysis of single video-frames of the switch-on and switch-off events in the CO^+ field ion image.

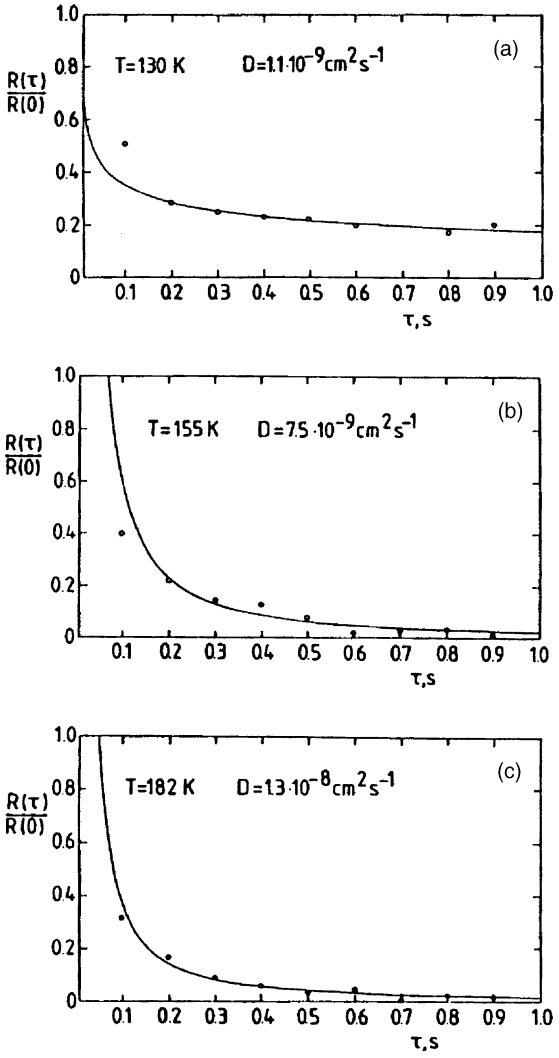

Fig. 13. Autocorrelation function, $R(t)/R(0)$, for the locally (probe–hole) measured CO^+ ion rate fluctuations at: (a) 130 K; (b) 155 K and (c) 182 K. (Solid lines) theoretical functions and (circles) experimental values [51].

Fig. 15 presents the temperature dependence (Arrhenius plot) of the diffusion coefficients, obtained with probing distances, as estimated above. The slope of this dependence yields a value of 0.12 eV for the activation energy of CO in a second, weakly bound layer. This value is in qualitative agreement with the diffusivities reported by Gomer for CO on CO/W and CO on CO/Pt, obtained from shadowing measurements [5]. To compare quantitatively present data with the results of [5], the different values of the applied field used in these two types of experiment should be

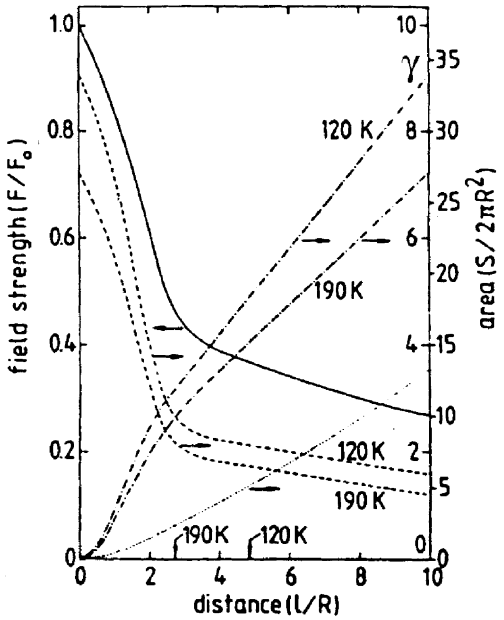

Fig. 14. Calculated dependence of asymptotic field strength F (solid line) and field enhancement of the CO gas-kinetic flux γ toward the surface (dashed lines) on distance from the top of the tip, L. Corresponding dependence on L of geometric surface area (dotted line) and effective surface area S (accounting for field enhancement of CO flux, dot-dashed line) are also displayed. Vertical arrows indicate limits of trapping zone for CO at 120 and 190 K, respectively. Externally applied field $F_0 = 20$ V/nm [51].

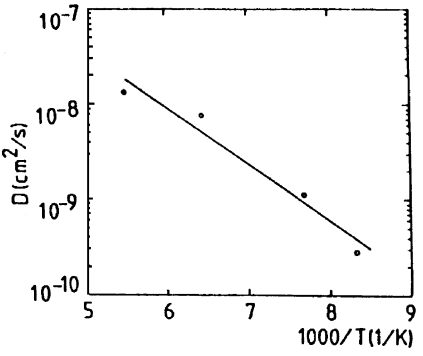

Fig. 15. Temperature dependence of diffusivity D of CO molecules on CO/W(1 1 1) at FIM experimental conditions ($p_{CO} = 2.0 \times 10^{-5}$ Torr, $F_0 = 20$ V/nm) [51].

taken into account. The results reported here are a first attempt to implement the DF method for examining reactive-gas diffusivity in the FIM. The critical experimental aspect of these measurements is the short observation time limited by the number of channels (1 0 2 4) in the applied analyzer. Hence, it appeared necessary to pass the

sample reading through a narrow band numerical filter. Since the extracted signal was used for calculating the AF it would be desirable to use a corresponding correction of the theoretical AF, as it was done for the FEM mode in Refs. [55,56]. Since such a correction has not yet been performed, this effects, of course, the accuracy of the obtained diffusivity data. Nevertheless, despite the rather qualitative significance of the obtained diffusivity numbers, the present experiments demonstrate the possibility of using the DF method for studying microscopic diffusion of imaging gases in FIM.

6. Concluding remarks and perspectives

The fluctuation approach of exploring various surface phenomena is by no means exhausted. New developments and problems, such as, e.g., the influence of intrinsic fluctuations on chemical kinetics are of both technological and scientific interest. The nanoscale dimensions of the ultrafine precious-metal pellets of commercial catalysts and the corresponding numbers of reacting particles on an average facet (10^2–10^4) force consideration the role of fluctuations in such reaction systems. Fluctuation effects, such as noise-induced transitions [57], can influence the nucleation and propagation of chemical waves, and are technologically related to catalytic ignition, extinction in catalytic reactions, instabilities in chemical reactors, and reaction rate-multiplicity [58]. The noise in the nanoscaled systems may lead to the various nontrivial effects, such as resonant activation [59], stochastic resonance [60], noise-induced stabilization [61] and synchronization [62]. Such effects are important not only in catalytic reaction systems, but also play a significant role in related fields, such as enzyme-governed membrane processes [63] or noise-improved signal transmission [64].

The widespread use of the scanning tunneling microscopy (STM), including its variable-temperature versions, and the significant progress in the development of the STM high-time resolution technique now enable DFs to be measured by monitoring STM tunneling current [65], thus contributing significantly to the range of the effects studied.

The FIM extension of the DF method has been recently successfully used for the first time to examine microscopic diffusion of molecules of a reactive imaging gas a FIM. This opens up new fields of investigations of SD in high field conditions, as well as during the in situ imaging of the surface reactions in the FIM.

The FEM fluctuation approach still has prospects as well: it had been demonstrated that a ''virtual probe–hole'' analysis of the digitized FEM images can be employed as an useful extension of the FEM fluctuation method. Compared to the conventional probe–hole technique, such an approach provides a means of measuring the temporal, as well as the spatial correlation of fast dynamic processes which are related to the DFs in the areas of any size chosen at any location on the imaged surface. So it becomes possible to follow up experimentally the theoretical predictions for ''overlapping'' or ''contacting'' probe–holes which are hardly realizable with conventional experimental techniques. Such interesting effects as diffu-

sion anisotropy, compressibility of adlayers, second-order phase transitions, already touched by the traditional probe–hole approach, can be studied via digitizing the FEM images, provided the main technical problem of the time resolution can be solved by the use of the high-speed video-cameras.

The technical problems are, of course, not the sole difficulty facing the fluctuation approach. Such basic problems as the finite resolution of the FEM/FIM/STM, the role of the boundary conditions or the anisotropy of the adsorbed layer, as well as the effect of the low- and high frequency cut-off are still challenges to the application of the DF method. These and other difficulties, which will appear during the development process, will not, in our conviction, diminish the belief that DFs in adsorbed layers are interesting and worthy of study.

Acknowledgements

The authors are deeply indebted to the late Professor Maria Stęślicka who brought J.B. and Y.S. together in 1990, during the 14th International Symposium on Surface Physics that she chaired. An enduring and fruitful cooperation was thus initiated, which made interesting joint projects possible, including the present work.

References

[1] A.G. Naumovets, Yu.S. Vedula, Surf. Sci. Rep. 4 (1985) 365;
A.G. Naumovets, Z. Zhang, Surf. Sci. 500 (2002) 414, and references therein.
[2] L. Onsager, Phys. Rev. 38 (1931) 2265, 38 (1931) 2265.
[3] Ch. Kleint, H.-J. Gasse, Z. Naturfor. 15a (1960) 87.
[4] R. Gomer, Surf. Sci. 38 (1973) 373.
[5] R. Gomer, Rep. Prog. Phys. 53 (1990) 917, and references therein.
[6] Y. Suchorski, J. Beben, R. Imbihl, Surf. Sci. Lett. 405 (1998) L477.
[7] V. Gorodetski, J.H. Block, W. Drachsel, M. Ehsasi, Surf. Sci. 67 (1993) 198;
Y. Suchorski, R. Imbihl, V.K. Medvedev, Surf. Sci. 401 (1998) 392.
[8] Y. Suchorski, J. Beben, R. Imbihl, Prog. Surf. Sci. 59 (1998) 343.
[9] J.-R. Chen, R. Gomer, Surf. Sci. 79 (1979) 413.
[10] M. Smoluchowski, Wien. Ber. 123 (1914) 2381.
[11] Ch. Kleint, Surf. Sci. 25 (1971) 394.
[12] A.M. Dabrowski, Ch. Kleint, Surf. Sci. 119 (1982) 118.
[13] E.S. Shikhovtseva, K. Skwarek, J. Beben, Surf. Sci. 317 (1994) 253.
[14] G. Mazenko, in: V.T. Bihn (Ed.), Surface Mobilities on Solid Materials, Plenum, New York, 1983, pp. 27–62.
[15] J. Beben, Ch. Kleint, R. Meclewski, Surf. Sci. 213 (1989) 438.
[16] D.R. Bowman, R. Gomer, K. Mutalib, M. Tringides, Surf. Sci. 138 (1984) 581.
[17] J. Beben, Solid State Phenom. 12 (1990) 17.
[18] J.-R. Chen, R. Gomer, Surf. Sci. 81 (1979) 589.
[19] Ch. Kleint, Phys. Stat. Sol. A 55 (1979) 447.
[20] M. Tringides, R. Gomer, Surf. Sci. 155 (1985) 254.
[21] R. DiFoggio, R. Gomer, Phys. Rev. B 52 (1982) 3490.
[22] D. Reed, G. Ehrlich, Surf. Sci. 105 (1981) 603.
[23] G.W. Timm, A. van der Ziel, Physica 32 (1966) 1333.

[24] M.A. Gesley, L.W. Swanson, Phys. Rev. B 32 (1985) 7703.
[25] J. Beben, Ch. Kleint, R. Meclewski, Z. Phys. B Cond. Matter 69 (1987) 319.
[26] Ch. Kleint, Surf. Sci. 25 (1971) 394, p. 411.
[27] J. Beben, Ch. Kleint, R. Meclewski, Physica 68 (1973) 382.
[28] J. Beben, Ch. Kleint, R. Meclewski, Surf. Sci. 93 (1980) 33.
[29] G.L. Kellogg, T.T. Tsong, P. Cowan, Surf. Sci. 70 (1978) 485.
[30] V.K. Medvedev, A.I. Jakivtshuk, Fiz. Tverd. Tela 16 (1974) 981.
[31] A. Sadiq, K. Binder, Surf. Sci. 128 (1983) 350.
[32] I.F. Luksyutov, A.G. Naumovets, V.L. Pokrovsky, Two-Dimensional Crystals, Academic Press, Boston, 1992.
[33] T. Biernat, Ch. Kleint, Appl. Phys. A 50 (1990) 95.
[34] V.K. Medvedev, A.G. Naumovets, T.P. Smereka, Surf. Sci. 34 (1973) 368.
[35] M. Tringides, R. Gomer, Surf. Sci. 166 (1986) 419.
[36] G. Mazenko, J.R. Banavar, R. Gomer, Surf. Sci. 107 (1981) 459.
[37] G. Doyen, G. Ertl, J. Chem. Phys. 62 (1975) 2957.
[38] W.G. Fan, A. Ignatiev, Phys. Rev. B 38 (1988) 366.
[39] M.S. Gupalo, Fiz. Tverd. Tela 22 (1980) 2311.
[40] M.F.H. van Tol, F.A. Hondsmerk, J.W. Bakker, B.E. Nieuwenhuys, Surf. Sci. 226 (1992) 529.
[41] M.C. Reckzgel, V. Gorodetski, J.H. Block, Appl. Surf. Sci. 94/95 (1996) 194.
[42] Y. Suchorski, J. Beben, R. Imbihl, Ultramicroscopy 73 (1998) 67.
[43] R. Gomer, A. Auerbach, Surf. Sci. 167 (1986) 493.
[44] Y. Suchorski, Act. Phys. Pol. A 81 (1992) 295.
[45] A.O. Snitko, Ukr. Phys. J. 36 (1991) 1561.
[46] T. Biernat, J. Beben, R. Meclewski, Surf. Sci. 266 (1992) 11.
[47] A.M. Dabrowski, Ch. Kleint, Surf. Sci. 172 (1986) 372.
[48] Y. Suchorski, J. Beben, E.W. James, J.W. Evans, R. Imbihl, Phys. Rev. Lett. 82 (1999) 1907.
[49] Y. Suchorski, W.A. Schmidt, N. Ernst, J.H. Block, H.J. Kreuzer, Prog. Surf. Sci. 48 (1995) 121, and references therein.
[50] W.A. Schmidt, Y. Suchorski, J.H. Block, H.J. Kreuzer, R.L.C. Wang, Surf. Sci. 326 (1995) 243.
[51] Y. Suchorski, J. Beben, V.K. Medvedev, J.H. Block, Appl. Surf. Sci. 94/95 (1996) 207.
[52] Y. Suchorski, W.A. Schmidt, J.H. Block, V.K. Medvedev, Surf. Sci. 331–333 (1995) 277.
[53] M.J. Southon, Ph.D. Thesis, Cambridge, 1963.
[54] V.K. Medvedev, N.N. Popovich, A.O. Snitko, Sov. Phys.-Tech. Phys. 36 (1991) 223.
[55] Y. Song, R. Gomer, Surf. Sci. 290 (1993) 1.
[56] J. Beben, W. Gubernator, Surf. Sci. 304 (1994) 59.
[57] Y. Suchorski, J. Beben, R. Imbihl, E.W. James, D.-J. Liu, J.W. Evans, Phys. Rev. B 63 (2001) 165417.
[58] M. Rinnemo, D. Kulginov, S. Johansson, K.L. Wong, V.P. Zhdanov, B. Kasemo, Surf. Sci. 376 (1997) 297.
[59] R.N. Mantegna, B. Spagnolo, Phys. Rev. Lett. 84 (2000) 3025.
[60] L. Gammiatoni, P. Hänggi, P. Jung, F. Marchesoni, Rev. Mod. Phys 70 (1998) 1.
[61] R. Wackerbauer, Phys. Rev. E 59 (1999) 2872.
[62] J. Feng, D. Brown, G. Li, Phys. Rev. E 61 (2000) 2987.
[63] A. Fulinski, J. Chem. Phys. 96 (1992) 3549.
[64] A. Fulinski, P.F. Gora, Phys. Rev. E 64 (2001) 011905.
[65] M.L. Losano, M.C. Tringides, Europhys. Lett. 30 (1995) 537.